

# CYCLIC RESPONSE OF RC BEAM-COLUMN JOINTS STRENGTHENED WITH TRANSVERSE STEEL BARS AND WITH C-FRP DIAGONAL TIES

EMMANOUIL GOLIAS<sup>a,\*</sup>, EMMANOUIL A. VOUGIOUKAS<sup>b</sup>, KLAUS WITTEMANN<sup>c</sup>,  
GEORGE I. KALOGEROPOULOS<sup>d</sup>, CHRIS KARAYANNIS<sup>a</sup>

<sup>a</sup> Democritus University of Thrace, School of Engineering, Civil Engineering Department, GR 67100 Xanthi, Greece

<sup>b</sup> National Technical University of Athens, School of Civil Engineering, Reinforced Concrete Laboratory, GR 15773 Athens, Greece

<sup>c</sup> Beratender Ingenieur, SLP Ingenieurbüro für Tragwerksplanung, Weinbrennerstr. 18, 76135 Karlsruhe, Germany

<sup>d</sup> Aristotle University of Thessaloniki, School of Engineering, Civil Engineering Department, Laboratory of Reinforced Concrete and Masonry Structures, GR 54124 Thessaloniki, Greece

\* corresponding author: [egkolias@civil.duth.gr](mailto:egkolias@civil.duth.gr)

**ABSTRACT.** The use of additional bars, internally placed through drill holes, in external beam-column connections subjected to cyclic loading, as shear reinforcement is experimentally investigated.

The presented experimental work includes tests of full-scale specimens with different reinforcement arrangements in the joint area, they are as follows: (a) the JB0V control specimen with two (extra) vertical side bars without shear reinforcement in the joint area and, (b) the JB0R joint, same as in the case of the control specimen, without the extra vertical bars, but with four additional steel bars that were placed in holes, which were drilled through the concrete of the joint body for this purpose, (c) the JB0VFX joint, the damaged control specimen repaired and strengthened with C-FRP diagonal ties (rope connections) through the joint area. The effectiveness of these additional bars and ropes as a shear reinforcement on the overall seismic performance of the tested joint is examined.

A comparison between the test results of the examined specimens indicated that the applied retrofitting technique is appropriate for the enhancement of the overall hysteretic performance of the beam-column joints in terms of load carrying capacity, stiffness and hysteretic energy dissipation.

**KEYWORDS:** R/C joints, repair and strengthening, CFRP ropes, cycling loading.

## 1. INTRODUCTION

Modern Codes' requirements for earthquake resistant structures are tighter than those a few decades ago. Several methods have been developed for upgrading the bearing capacity of existing concrete-framed buildings, the majority of which has been constructed according to elementary earthquake resistant provisions. Strengthening of existing structural members is usually necessary in most cases in order to reach modern demands in earthquake engineering, as reported by researchers, e.g., Cosenza et al. [1], and National structural codes and recommendations, e.g., EPANTYK [2].

Though several efficient methods are applied for the strengthening of existing linear members, there are many limitations for the upgrade of the capacity of existing nodes, mainly due to practical reasons. Nevertheless, increasing the capacity of linear members, without analogous provisions for the capacity of the nodes, attenuates the ability to improve the whole structure's capacity. As no specific rules had been established for shear reinforcement in the joint areas until about four decades ago, it was not rare that

nodes were constructed with sparse, or even lack of stirrups.

The first structural attempts for strengthening of such existing nodes (with "poor" detailing), included jacketing, either with the use of steel plates, or shotcrete [3–7]. If a node had been lightly damaged, epoxy resin injections were used before jacketing [8]. Alternatively, adding steel collars have been proposed [9].

Introduction of the FRPs at the beginning of the new century led to the development of related techniques that have, gradually, substituted the older techniques that were labour intensive and increased the structural elements' dimensions [10]. Applications of externally applied FRPs have been studied for over 20 years by many researchers, due to their advantages [11]. An analytical review of state-of-the-art interventions to RC beam column joints with FRP has been also reported [12]. As the majority of the nodes are surrounded by 3 or 4 beams, abovementioned interventions require complex and expensive techniques for their application.

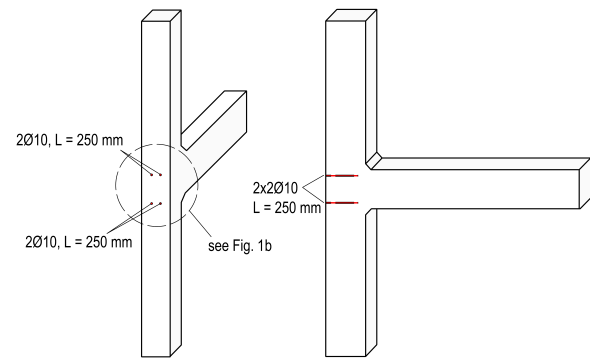
A novel technique has been proposed recently, so that both the complexity and the cost of nodes' restoration or/and strengthening can be reduced. In recent experimental techniques [13–17], external FRP flexural ropes have been used as an additional diagonal reinforcement to existing beam column joints. This type of reinforcement is encapsulated in U-shaped notches.

Focused on the use of flexural FRP ropes, the present paper deals with the performance of type “T” nodes, strengthened with CFRP bars, placed in their position through drilling, and subjected to cyclic loading. A direct comparison of results between an unstrengthened (initial) specimen, specimen strengthened in a conventional manner, and specimen strengthened through drilling, shows positive results for the examined node strengthening method (through drilling).

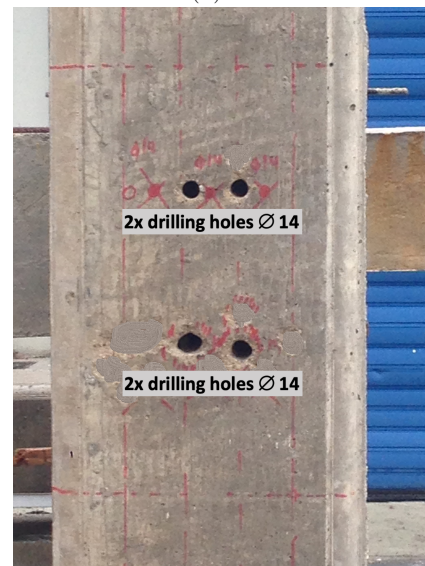
## 2. DESIGN OF SPECIMENS

The use of additional bars, internally placed through drill holes in external beam-column connections subjected to cyclic loading, as shear reinforcement is experimentally investigated. The presented experimental work includes tests of full-scale specimens with different reinforcement arrangements in the joint area.

The effectiveness of additional bars and ropes as shear reinforcement on the overall seismic performance of tested joints has been examined. To simulate an earthquake and the resulting loads, the unreinforced specimen JB0V was first subjected to cyclic loading on the test rig. Subsequently, the test specimen JB0R, reinforced with  $2\text{Ø}10$ ,  $L = 25$  cm at the top and bottom, was subjected to identical cyclic loads on the test rig. The reinforcing bars were placed as shown in Figure 1. Afterwards, the specimen JB0V, pre-damaged by the first test, had been reinforced with C-FRP ropes connections in the nodal region and again subjected to the identical cyclic loads on the test rig, labelled as JB0VFX. The results were digitally acquired and recorded using the measurement technique described, in more detail, in section 4.1. The geometry of the test specimens was chosen based on frequently occurring buildings in frame-and-transom constructions (floor height  $\approx 2.95$  m, beam length =  $0.5 \times$  room width  $\approx 2.0$  m). Then, a simulated cyclic earthquake load was applied to the test specimens on the test rig in a deformation-controlled manner. In the first four steps, the deformation rate was  $0.5$  mm/s and then increased to  $1$  mm/s. The longitudinal reinforcement of the column consisted of  $1\text{Ø}14$  in each corner and  $1\text{Ø}12$  in the centre of each side. As a shear reinforcement of the column,  $\text{Ø}8/10$  cm stirrups were arranged. The downstand beam was reinforced with  $4\text{Ø}14$  in the top and bottom layers and  $\text{Ø}8/10$  cm stirrups. The column had a cross-section of  $b/d = 250$  mm/ $350$  mm and a total length of  $L = 2.95$  m, the downstand beam had a cross-section of  $b/h = 250$  mm/ $350$  mm. The



(A).



(B).

FIGURE 1. Reinforcement of additional bars for model JB0R.

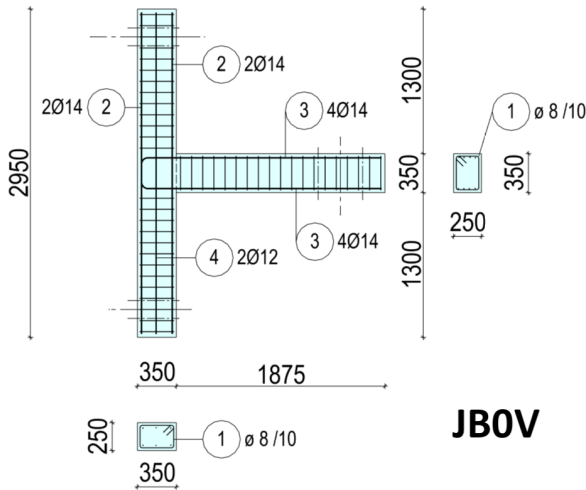


FIGURE 2. Geometry and reinforcement of initial model JB0V.

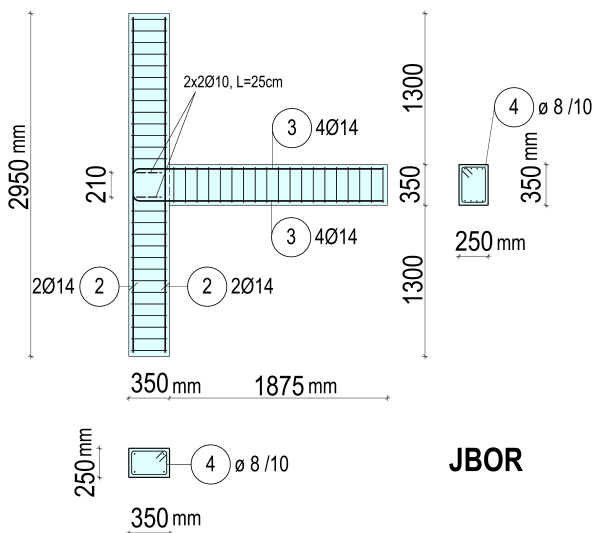
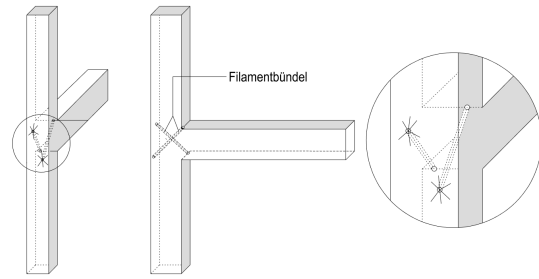


FIGURE 3. Geometry and reinforcement of initial model JB0R.

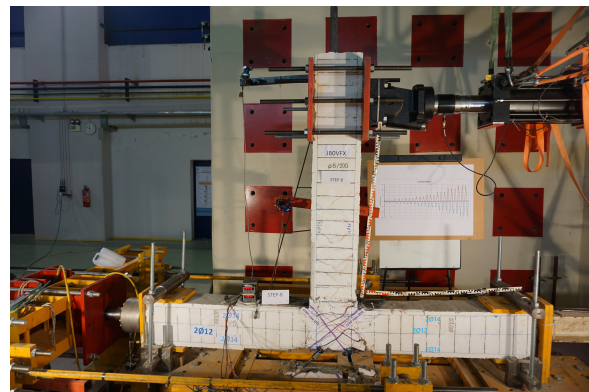
geometry, bending shape and location of the reinforcement are presented in Figure 2 and 3. The 28-day concrete compressive strength of the specimens was determined on cylindrical specimens of dimensions  $D \times h = 150 \text{ mm} \times 300 \text{ mm}$  at  $f_{cm} = 34 \text{ MPa}$ . A total of 9 cylindrical specimens were tested to determine the concrete compressive strength from a total of 16 test specimens. The value  $f_{cm} = 34 \text{ MPa}$  is the calculated average value of the compressive strength test. The steel grade of the reinforcing bars was B500S (B) bar steel with a yield strength of  $f_{yk} = 500 \text{ MPa}$ .

### 3. STRENGTHENING TECHNIQUES FOR FRAME NODES

Strengthening of the node of specimen JB0R has been performed prior to the tests. Holes  $\text{Ø}14 \text{ mm}$ ,  $L=250 \text{ mm}$  were drilled at  $0^\circ$  into the test specimen JB0R to be reinforced (Figure 1a and 1b). The drill



(A) . Strengthened specimen JB0VFX C-FRP rope.



(B) . Reinforcement of additional bars for model JB0R.

FIGURE 4.

holes were cleaned with compressed air to remove drill dust and debris.

Sika Anchorfix-3+ was then injected into the boreholes and the  $\text{Ø}10$  round steel reinforcement pre-impregnated with Sikadur-52 was inserted into the boreholes.

After cyclic loading of the test specimen JB0V, the damage was caused in the nodal area (Figure 4a). Loose concrete parts were first removed. Then, the damaged area was shuttered and grouted with Sika Monotop-34. During this process, C-FRP rope bundles, diagonally impregnated with Sikadur-52, were tightly installed and fixed to improve the shear force bearing capacity. The C-FRP ropes are high-strength plastics that act as ropes and can transfer high tensile forces. Details on these materials can be found in Table 1. The damaged specimen JB0V has been repaired and strengthened with C-FRP ropes crossing the node diagonally (Figure 4a and 4b). The first rope has been placed starting from the bottom back of the node and wound towards the upper face of the existing beam; the second rope started from the top back of the node and wound towards the upper face of the existing beam (Figure 4). The fixed specimen was labelled as JB0VFX. It was then subjected to the identical cyclic loads on the test rig again. The performance of the two test specimens is evaluated and compared.

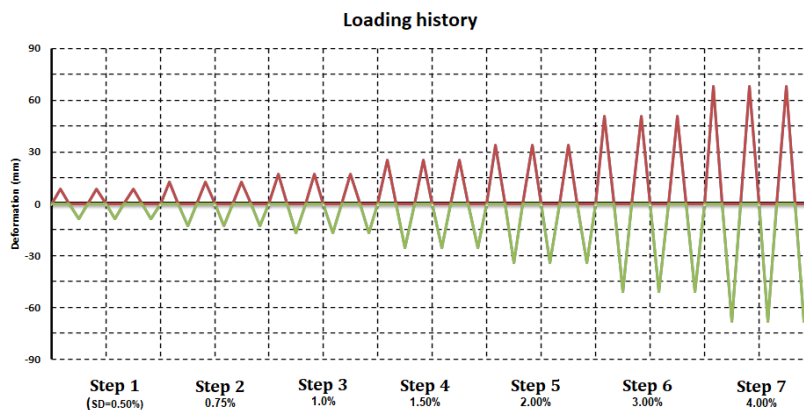


FIGURE 5. Loading sequence.

Material	$E$ [Gpa]	$f$ [MPa]	$\varepsilon_{max}$ [%]
C-FRP	240	4000	1,6
Anchorfix-3+	n/a	114	>1,6
Sikadur-52	1,8	37	>1,6

TABLE 1. Properties of materials used for repair and strengthening.

The final anchoring of the rope ends is done in a star shape in milled slots. The Sika Anchorfix-3+ is then placed in the slots and the C-FRP ropes impregnated with Sikadur-52 has been casted. The properties of the materials used are given in Table 1.

## 4. EXPERIMENTAL PROGRAM

### 4.1. TEST SETUP AND INSTRUMENTATION

Properties of materials used are given in Table 1. The test rig and the measuring equipment used are shown in Figure 5. The test specimen was installed rotated by  $90^\circ$  so that the downstand beam pointed vertically upwards. The support was horizontal. By means of special support devices, free rotation of the frame node was made possible. This allows the position of the turning points to be moved to the centre of the supports, thus simulating an analogous frame construction. The support of the test specimen was constantly loaded with an axial normal force  $\nu_c = N_c/A_c f_{cm} \approx 0.05$  during the entire test run. An axial normal force  $\nu_c = N_c/A_c f_{cm} < 0.05$  would result in unrealistic nodal loading. In reality, such frame constructions are loaded with a related axial normal force  $\nu_c = N_c/A_c f_{cm} \geq 0.05$ , so that a conservative lower value of  $\nu_c = 5\text{--}10\%$  is usually used as a basis for experiments. For loading the test specimens, a hydraulic piston was used, which was placed at a distance of 1.475 m from the side of the beam at the free end of the beam. The piston was equipped with a load cell screwed into its front part, while internally it was equipped with a linear differential displacement counter (LVDT). The piston was connected to a dig-

ital control unit to selectively apply a displacement or force to the piston under a precise software control. Thus, the force amplification command leads to the piston movement with parallel dense control (in short intervals) of the display of the force meter integrated in the piston. With the approach of the command, the program sends a signal for a small increase or decrease of the force until a predetermined accuracy is achieved in this step. Similarly, switching operations were also performed, which were recorded, checked and corrected with a displacement meter integrated in the piston. This digital control system was also used to record and store readings from external instruments, which could additionally act as experimental control instruments. The software used to perform the experiment was the M.T.S. Teststar software package. In addition to the piston used to apply the horizontal displacement, a second hydraulic piston was used, which was attached to the left end of the support. This was used to apply the support compression force, which remained constant throughout the experimental process ( $N_c = 0.05 \times A_c \times f_{cm} = 122.5$  kN).

Through the piston, the applied load was measured using a 0.025 kN precision load cell, while by using a linear 100 mm LVDT-A tensiometer, any spontaneous displacement of the test specimens was checked and taken into account in each load step. Additional cord displacement transducers SAA and SAE were attached to measure the displacements in this area and estimate the shear deformation. Figure 5 shows the described test setup.

### 4.2. LOADING

During the test, the specimen was subjected to a full cyclic deformation. The piston for deforming the test specimen engaged at the free vertical end of the beam (Figure 6). The lever arm for generating the moment at the node was 1.475 m. The specimen was loaded in seven load steps with increasing applied deformation of  $\pm 8.5$  mm,  $\pm 12.75$  mm,  $\pm 17$  mm,  $\pm 25.5$  mm,  $\pm 34$  mm,  $\pm 51$  mm and  $\pm 68$  mm (corresponding to storey drift (SD) from 0,50–4,00 %). Within each loading level, the deformation was applied with 3 repetitions, each in

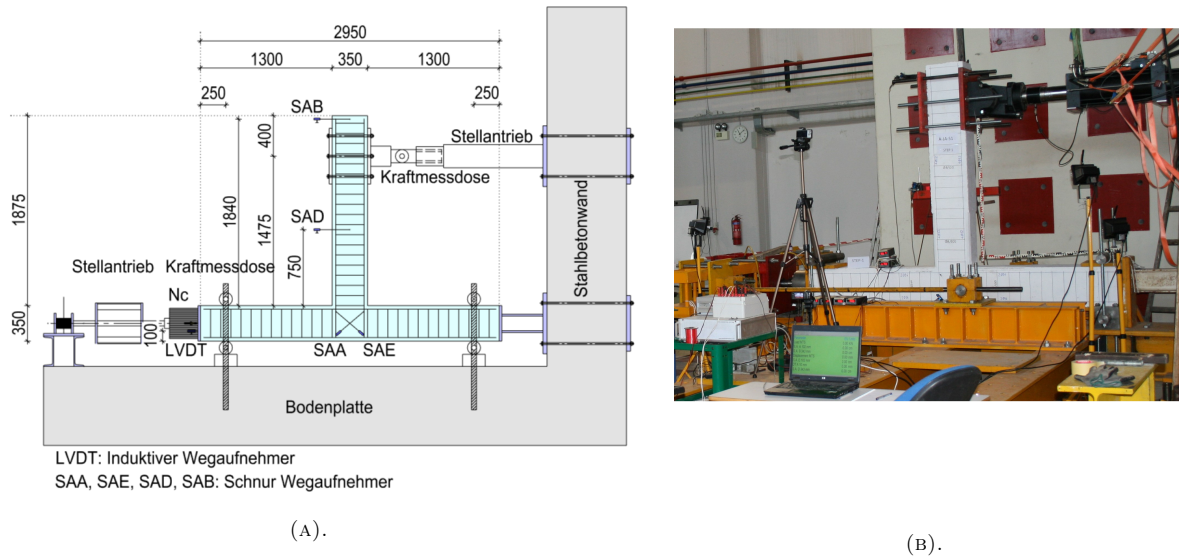


FIGURE 6. Test setup and instrumentation.

positive and negative direction. The loading sequence can be seen in Figure 5. In large-scale tests on reinforced concrete components, it is of great importance to select the load intensity and load control in such a way that both the ultimate limit state/capacity of the test specimen and the expected actions due to earthquakes are adequately covered. In the case of simulated earthquake loads with deformations in the plastic range, the load-bearing capacity, component resistance, and action cannot be considered separately from each other, since they are strongly dependent on each other. The basic parameters for determining the capacity curve of a component are strength, stiffness, inelastic deformation capacity (ductility) and, in addition, cumulative damage capacity parameters such as energy dissipation.

All of these parameters are expected to deteriorate as the number of damage cycles and the amplitude/intensity of the cycles in the test increase. Any loading of the component beyond the elastic regime will cause a permanent damage to the component and, usually, a permanent plastic deformation. In the load sequence on which this study is based, the emphasis was deliberately placed on load levels with several load changes within each intensity level, since repeated load cycles cause a damage pattern such as is frequently found in moderate earthquake loading. In order to be able to draw meaningful conclusions from the damage patterns occurring in each case, 3 repetitions were selected for each load level, each with the same deflections within the same level. After 3 repetitions, the load was then increased by applying the next larger deformation, again in 3 cycles of equal deflection.

In severe earthquakes, the intensity and type of loads applied to individual building components do not follow a consistent pattern. With increasing deformations, the number of loading cycles outside the elastic

range increases. At the same time, the vibration time of a building component increases. For structural components with a large initial stiffness, deformation states with stresses in the inelastic range occur very early. It is easy to see that the behaviour of a structure depends on a large number of variables. A single load sequence is, therefore, always a compromise or an approximation. The intensity of the load must be chosen so that it is conservative for most practical applications. In our experiment, this was achieved by a loading sequence of seven steps consisting of three cycles each (Figure 5).

A damage index was also included in the evaluation of the tests. The damage index introduced by Park and Ang (1985) was chosen in order to be able to compare the existing capacity (capacity for energy dissipation) of the existing nodal connection with reinforcement and the capacity of the same nodal connection without reinforcement.

### 4.3. EXPERIMENTAL RESULTS

In order to determine the effectiveness of the applied reinforcement method, the load-bearing capacity of the unreinforced specimen JB0V is compared with the load-bearing capacity of the reinforced specimens JB0R and JB0VFX. The hysteresis loops of the respective specimens are shown in Figure 7 by means of a force-displacement curves.

In the diagram, the dashed red lines represent the test results of the unreinforced specimen (JB0V), while the solid blue and green lines represent the results of the subsequently reinforced specimens JB0R and JB0VFX.

The comparison of the test results shows that the applied reinforcement method using 2Ø10 round steel reinforcement at the top and bottom increases the load capacity by only about 6%. The reinforcement by C-FRP ropes shows a significant improvement. The

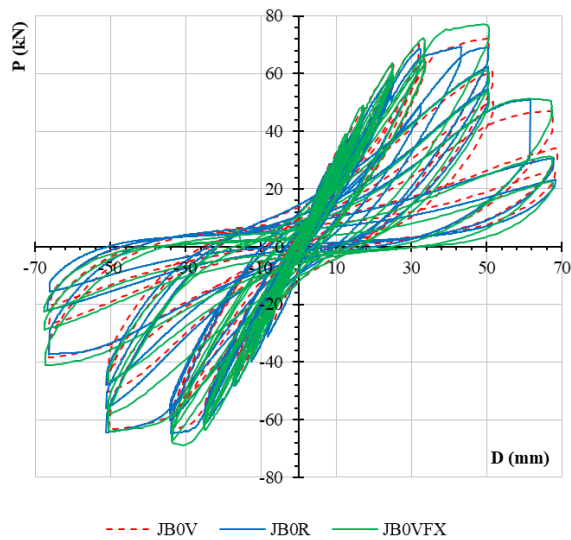


FIGURE 7. Force-displacement curves for all specimens.

damage patterns on the unreinforced specimen and the reinforced specimens after completion of the tests are compared in Figure 8. As can be seen, the damage pattern of both test specimens JB0V and JB0R is almost identical.

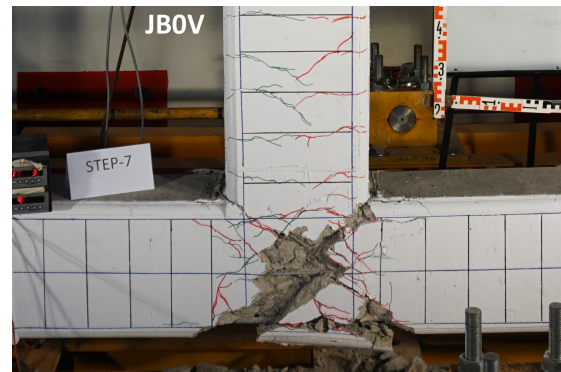
When reinforced with C-FRP ropes, the behaviour of the specimen JB0VFX is much more benign, the spalling of the concrete is greatly reduced, which is due to the fact that the rope reinforcement shows its effectiveness. This is also mainly due to the better anchorage of the C-FRP ropes adjacent to the highly stressed intersection. Thus, the overall damage pattern is significantly improved. The envelopes of the hysteresis loops for a full test run with 3 cyclic repetitions per loading level are shown in Figure 9a, 9b and 9c for all specimens, for all 3 cycles (seven steps per cycle).

In the diagrams, the test load ( $P$ ) required for the selected deformation is plotted against the relative displacement ( $SD$  – story drift). For the sake of better representability, only values up to a load level 7 with  $SD = 4\%$  and a displacement of  $\pm 68$  mm are plotted. In addition, Figure 10 shows the change in stiffness regarding to load levels. The dashed red line corresponds to the unreinforced specimen JB0V, the solid blue line to the reinforced specimen JB0R and the solid green line to the reinforced specimen JB0VF.

## 5. EVALUATION OF RESULTS

### 5.1. DAMAGE INDEX

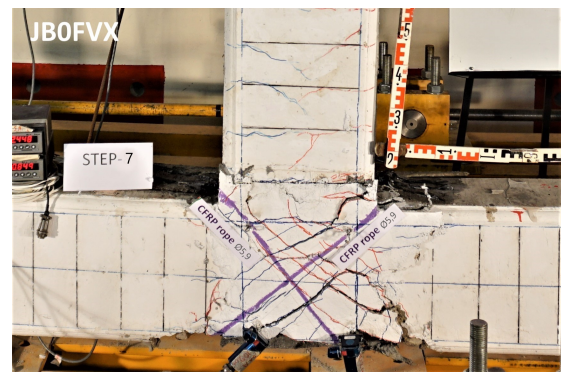
In the literature, several dimensionless evaluation methods are reported for assessing the damage of reinforced concrete elements after these elements have been subjected to loading outside the elastic regime. Most of these damage indices consider the damage of individual elements and are based on the plot of deformations and hysteresis curves with dissipated energy information. The damage index model of Park and



(A) . Final damage mode, specimen JB0V.



(B) . Final damage mode, specimen JB0R.



(C) . Final damage mode, specimen JB0VFX.

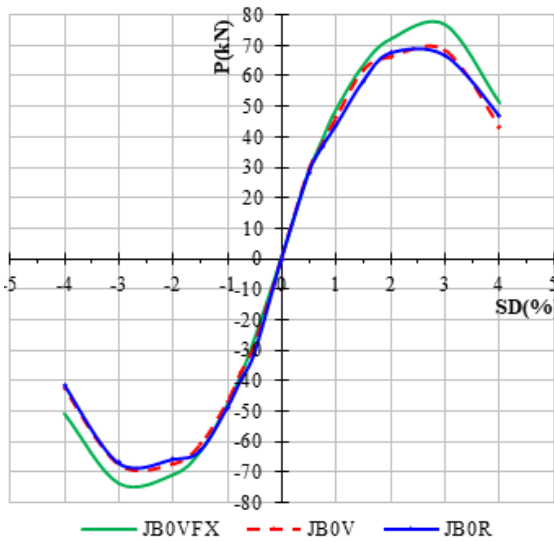
FIGURE 8.

Ang [18] has been widely applied in recent years, due to its simplicity and the fact that it has been calibrated with experimental data from different structures damaged during actual earthquakes.

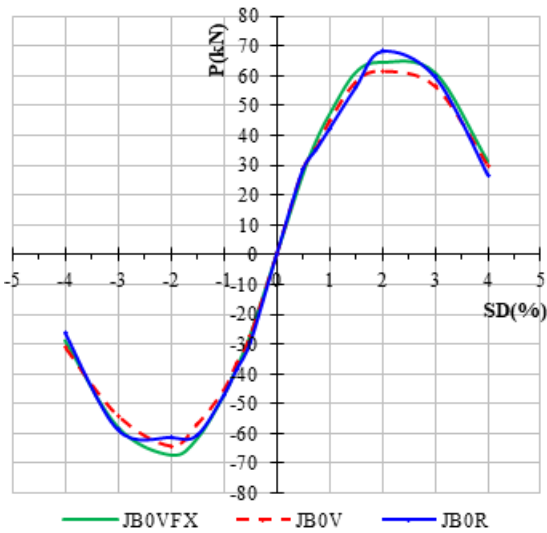
The damage index is defined as a linear combination of the final displacement and the dissipated energy as:

$$D = \frac{\delta_M}{\delta_u} + \frac{\beta}{M_y \delta_u} \int dE \quad (1)$$

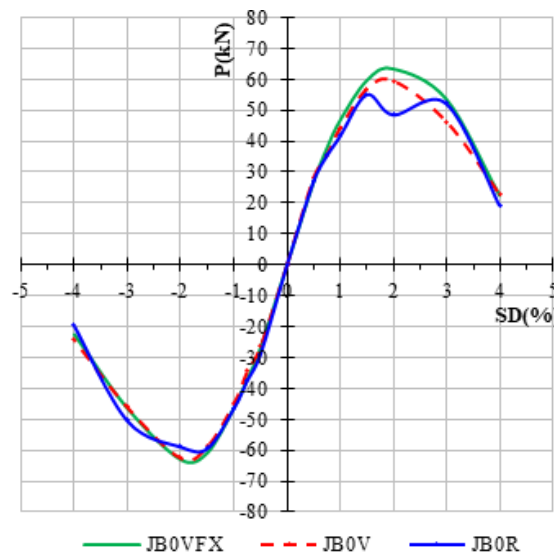
where  $\delta_M$ , represents the maximum deflection reached during seismic loading,  $\delta_u$  is the maximum deformation capacity under static load,  $\beta$  is a model parameter, depending on the transverse and normal forces, the longitudinal reinforcement ratio and the reinforcement layout.  $M_y$  is the calculated yield strength and  $dE$  is the incremental dissipated hysteretic energy. In the



(A) . Envelope curves of maximum loads at 1<sup>st</sup> loading cycles.

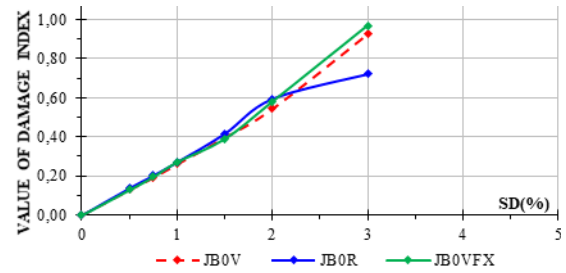


(B) . Envelopes of maximum loads at 2<sup>nd</sup> loading cycles.

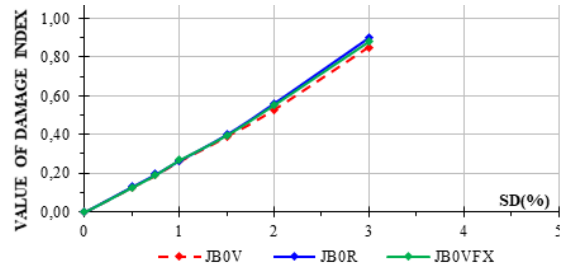


(C) . Envelopes of maximum loads at 3<sup>rd</sup> loading cycles.

FIGURE 9.



(A) . Damage index values for the 1<sup>st</sup> cycles of the loading steps.



(B) . Damage index values for the 3<sup>rd</sup> cycles of the loading steps.

FIGURE 10.

present study, the described damage index model of Park and Ang (1985) is used to draw objective conclusions for the effectiveness of the described repair procedure for the column-transom node and to determine the degree of damage of the test specimens for each load step.

The values of  $\delta_M$ ,  $M_y$ , and  $dE$  of this model were obtained from the test results, while the value of  $\delta_u$  was estimated using an empirical formula for calculating ultimate drift according to Eurocode 8 (EN 1998-1). Extensive tests have shown that for the quantitative estimation of the coefficient  $\beta$ , a value between 0.3 and 1.2 and a mean value of about 0.15 can be applied, as indicated by Cosenza et al. (1993). It should be noted that the value  $\beta = 0.15$  correlates very well with the results of other damage models and that this value has, therefore, been adopted very frequently by other researchers. The stiffness degradation of the specimens is presented in Figure 11. The values of the damage indices thus calculated on the basis of the model described above are given for the three specimens tested in Figure 10a and 10b, for all specimens, after 1 and 3 loading cycles, respectively.

### 5.2. EQUIVALENT VISCOUS DAMPING

In addition to the damage index, equivalent viscous damping is another good indicator of energy dissipation capacity per load cycle. The energy dissipation value determines the cyclic capacity of the specimen stressed to failure and defines the total energy that can be dissipated before the loss of system stability. The plastic deformations that occur after the specimen leaves the elastic region result in energy dissipation, which can be interpreted as additional damping. Figure 12 shows a general force-displacement diagram

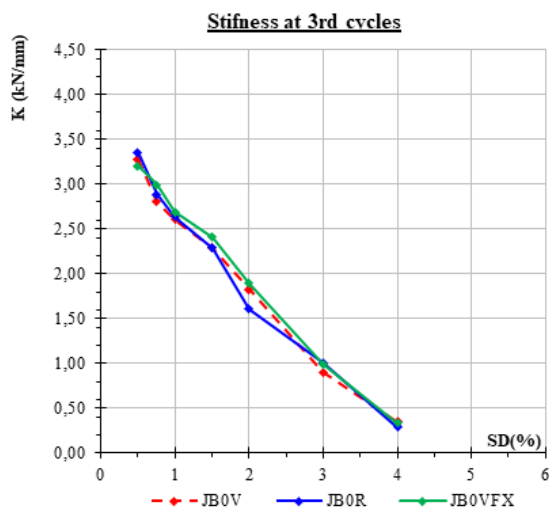


FIGURE 11. Stiffness degradation to load level.

under cyclic loading. Depending on the node formation in the area of the column/beam, the curve can vary accordingly. The hatched (crossed-out) area exemplarily represents the inelastic energy ( $W_{hyst}$ ) dissipated in the 1st loading interval of the 5th load level of specimen JB0R due to plastic deformations in the node. Obviously, the greater the ductility and thus the plastic deformation capacity of the materials, the greater is the integral of the hatched area, i.e., the energy enclosed by a hysteresis loop, and consequently the greater is the dissipated energy and thus the equivalent damping. The maximum elastic strain energy ( $W_{el}$ ), which corresponds to the depicted degree of deformation, is equal to the area of the triangle OAB.

The additional dissipation-induced damping can be expressed in terms of viscous damping, for which the following equivalent hysteresis damping ratio is commonly used:

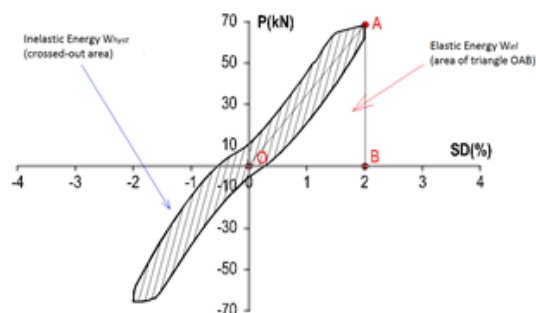
$$\zeta_{eq} = \frac{1}{4\pi} \cdot \frac{W_{hyst}}{W_{el}} \quad (2)$$

Based on the equivalent viscous damping  $\zeta_{eq}$ , useful conclusions can be drawn about the efficiency of the investigated reinforcement measure with respect to the energy dissipation capability of the nodal formation.

The dissipated energy of the three tests is captured in terms of equivalent viscous damping (Figure 13). Viscous damping of unreinforced and reinforced specimens is compared. The representation includes the first load cycle of all load steps of an overall test (again up to  $SD = 4\%$ ).

## 6. CONCLUSIONS

Comparing the abovementioned results, it can be stated that the energy dissipation capacity of the reinforced specimen (JB0R) is initially almost the same as that of the unreinforced specimen (JB0V) in the lower load levels. This can be easily explained by the fact that the bonded reinforcing bars have probably not yet been stressed into the plastic range, so the node



Hysteresis inelastic energy:  $W_{hyst} = 1077,24 \text{ kNmm}$   
 Maximum elastic energy:  $W_{el} = 1173,0 \text{ kNmm}$   
 Hysteresis damp. ratio:  $\zeta_{eq} = \frac{1}{4\pi} \cdot \frac{W_{hyst}}{W_{el}} = 0.073$

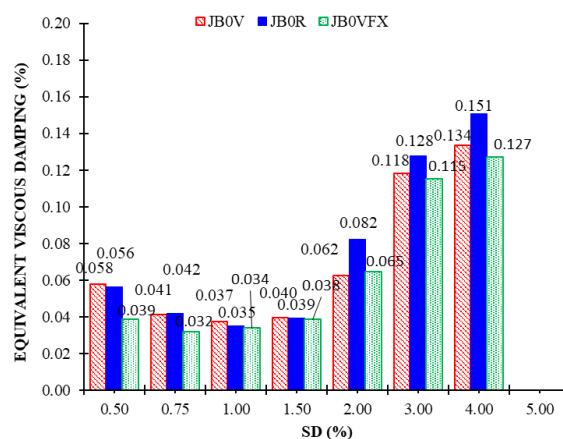
FIGURE 12. Hysteresis loop of the 1<sup>st</sup> loading cycle of the 5<sup>th</sup> loading step of the specimen JB0R.

FIGURE 13. Equivalent viscous damping, per loading level, for all 3 tested specimens.

with the reinforcement behaves similarly to the unreinforced one. Initially, the still low stress on the reinforcing bars does not cause a noticeable increase in dissipation ( $SD$  up to 1.50%, Figure 13). With a further load increase, the damage increases, diagonal cracks form and the bonded reinforcing bars jump. This can be observed for load steps 5–8 ( $SD$  from 2–4%), where the reinforced specimen shows a clear, though not too large, increase in energy dissipation capacity as compared to the unreinforced specimen.

Authors would have expected a more significant increase, but the fact that this did not occur is attributed to the cause that the glued-in bars are probably too short to be sufficiently anchored. If one looks at the crack formation and assumes a basic anchorage length of a  $\varnothing 10$  mm rebar of approx. 32 cm, only a few centimetres were anchored behind the crack flank. It is well known that cyclic loads lead to a very high stress on the anchorage areas anyway, since micro-crack formation and the surrounding local tension fields in the anchorage area give rise to the possibility of premature slippage of the reinforcing bar.

For a future investigation, it is recommended to provide the reinforcement bars with at least an anchorage length  $l_b$  in the frame ledger. Also, to provide an additional end anchorage at the column, for example, by means of external, welded square anchor plates. The latter would also hinder spalling of the bottom concrete cover, which can be observed at the lower part of Figure 8c. Since gluing in straight reinforcing bars does not cause any major problems and can also be realized comparatively inexpensively, it is recommended that the node be penetrated with considerably more reinforcement, which must be anchored very carefully in accordance with the aforementioned recommendation.

## REFERENCES

- [1] E. Cosenza, G. Manfredi, G. M. Verderame. Seismic assessment of gravity load designed R.C. frames: Critical issues in structural modelling. *Journal of Earthquake Engineering* **6**(sup001):101–122, 2002. <https://doi.org/10.1080/13632460209350434>.
- [2] Structural recommendations (2006) EPANTYK, a National Greek program for the seismic assessment of existing buildings (in Greek), TEE; Athens, Greece, 2006. <https://docplayer.gr/38084025-Synoptiki-paroysiassi-raseon-epantyk-ethniko-prograua-antiseisukis-enishysis-yfistauenon-kataskeyon.html>.
- [3] S. M. Alcocer. Rehabilitation of RC frame connections using jacketing. In *10th World Conference Earthquake Engineering*, pp. 5235–5240. 1993. [https://www.iitk.ac.in/nicee/wcee/article/10\\_vol9\\_5235.pdf](https://www.iitk.ac.in/nicee/wcee/article/10_vol9_5235.pdf).
- [4] R. S. Aboutaha, M. D. Engelhardt, J. O. Jirsa, M. E. Kreger. Retrofit of concrete columns with inadequate lap splices by the use of rectangular steel jackets. *Earthquake Spectra* **12**(4):693–714, 1996. <https://doi.org/10.1193/1.1585906>.
- [5] A. Biddah, A. Ghobarah, T. S. Aziz. Upgrading of nonductile reinforced concrete frame connections. *Journal of Structural Engineering* **123**(8):1001–1010, 1997. [https://doi.org/10.1061/\(ASCE\)0733-9445\(1997\)123:8\(1001\)](https://doi.org/10.1061/(ASCE)0733-9445(1997)123:8(1001)).
- [6] A. Ghobarah, A. Biddah, M. Mahgoub. Rehabilitation of reinforced concrete columns using corrugated steel jacketing. *Journal of Earthquake Engineering* **1**(4):651–673, 1997. <https://doi.org/10.1080/13632469708962382>.
- [7] A. G. Tsonos. Lateral load response of strengthened reinforced concrete beam-to-column joints. *ACI Structural Journal* **96**(1):46–56, 1999. <https://doi.org/10.14359/595>.
- [8] C. G. Karayannis, C. E. Chalioris, K. K. Sideris. Effectiveness of RC beam-column connection repair using epoxy resin injections. *Journal of Earthquake Engineering* **2**(2):217–240, 1998. <https://doi.org/10.1080/13632469809350320>.
- [9] A.-D. G. Tsonos. A new method for earthquake strengthening of old R/C structures without the use of conventional reinforcement. *Structural Engineering and Mechanics* **52**(2):391–403, 2014. <https://doi.org/10.12989/SEM.2014.52.2.391>.
- [10] M. Engindeniz, L. F. Kahn, A.-H. Zureick. Repair and strengthening of reinforced concrete beam-column joints: State of the art. *ACI Structural Journal* **102**(2):187–197, 2005. <https://doi.org/10.14359/14269>.
- [11] G. Kalogeropoulos, A.-D. Tsonos. Cyclic performance of RC columns with inadequate lap splices strengthened with CFRP jackets. *Fibers* **8**(6):39, 2020. <https://doi.org/10.3390/fib8060039>.
- [12] D. A. Pohoryles, J. Melo, T. Rossetto, et al. Seismic retrofit schemes with FRP for deficient RC beam-column joints: State-of-the-art review. *Journal of Composites for Construction* **23**(4):03119001, 2019. [https://doi.org/10.1061/\(ASCE\)CC.1943-5614.0000950](https://doi.org/10.1061/(ASCE)CC.1943-5614.0000950).
- [13] E. Golias, H. Lindenthal, F.-H. Schlüter, A. I. Karabinis. Ertüchtigung seismisch beschädigter Rahmenknoten aus Stahlbeton mittels FRP-Filamentbündelverbindungen. *Bautechnik* **97**(4):268–278, 2020. <https://doi.org/10.1002/bate.201900085>.
- [14] E. Golias, A. G. Zapris, V. K. Kytinou, et al. Application of X-shaped CFRP ropes for structural upgrading of reinforced concrete beam-column joints under cyclic loading – Experimental study. *Fibers* **9**(7):42, 2021. <https://doi.org/10.3390/fib9070042>.
- [15] C. G. Karayannis, E. Golias. Strengthening of deficient RC joints with diagonally placed external C-FRP ropes. *Earthquakes and Structures* **20**(1):123–132, 2021. <https://doi.org/10.12989/eas.2021.20.1.123>.
- [16] C. G. Karayannis, E. Golias. Full-scale experimental testing of RC beam-column joints strengthened using CFRP ropes as external reinforcement. *Engineering Structures* **250**:113305, 2022. <https://doi.org/10.1016/j.engstruct.2021.113305>.
- [17] E. Golias, A. G. Zapris, V. K. Kytinou, et al. Effectiveness of the novel rehabilitation method of seismically damaged RC joints using C-FRP ropes and comparison with widely applied method using C-FRP sheets – Experimental investigation. *Sustainability* **13**(11):6454, 2021. <https://doi.org/10.3390/su13116454>.
- [18] Y.-J. Park, A. H.-S. Ang. Mechanistic seismic damage model for reinforced concrete. *Journal of Structural Engineering* **111**(4):722–739, 1985. [https://doi.org/10.1061/\(ASCE\)0733-9445\(1985\)111:4\(722\)](https://doi.org/10.1061/(ASCE)0733-9445(1985)111:4(722)).